Desalination and Water Treatment
www.deswater.com

doi: 10.5004/dwt.2018.22428

129 (2018) 289–298
October

Research on construction of land surface temperature/vegetation index feature space

Xinghan Wang[a,b,c,*], Peitong Cong[b], Chaoqun Liu[a], Xiaogang Wang[a]

[a]*Pearl River Institute of Hydraulic Research, Pearl River Water Resources Commission, Ministry of Water Resources, Guangzhou, China*
[b]*College of Water Conservancy and Civil Engineering, South China Agriculture University, Guangzhou, China; email: rsgiswxh@126.com (X. Wang)*
[c]*Key Laboratory of the Pearl River Estuarine Dynamics and Associated Process Regulation, Ministry of Water Resources, Guangzhou, China*

Received 7 August 2017; Accepted 29 April 2018

ABSTRACT

The land surface temperature/vegetation index feature space has important application in quantitative soil remote sensing inversion and drought monitoring, water resources management, such as soil water content, evapotranspiration. However, the study of its feature space construction method is still relatively lacking. In this study, we take the Oklahoma state of the United States as an example, the fitting method of the dry and wet edges of the land surface temperature/vegetation index feature space is carried out, and the linear and index, logarithm, polynomial, and power functions are used to fit the dry and wet edges, respectively, and the fitting results were evaluated by the measured soil water content data. We found that the results by polynomial function fitting, *r*-squared is the highest in the five fitting modes, and *r*-squared is more than 0.66 in the dry and wet edges of the feature space; and the water content of soil surface was compared with that of soil moisture content, and the root mean square error value is the smallest. In conclusion, these results strongly suggest that the polynomial function fitting the dry and the wet edges is the best way to construct the land surface temperature/vegetation index feature space.

Keywords: Land surface temperature; Vegetation index; Feature space; Dry edge; Wet edge

1. Introduction

The land surface temperature (LST)/vegetation index feature space is an interpretation of the two-dimensional spatial distribution of surface radiation temperature and fractional vegetation cover [1]. The feature space used for soil moisture and evapotranspiration estimates begins with the discovery of Price [1,2], when the fractional vegetation cover and soil wet and dry extent span are large, the scatter plot of the remote sensing vegetation index and the LST is approximately triangular, it consists of two extreme boundaries; one is dry, represents a serious water deficit, no moisture can be used for evapotranspiration; the other is wet side, on behalf of the soil water is sufficient, the vegetation is in a potential evapotranspiration state. In the early study, the researchers found a strong correlation between the remote sensing spectral vegetation index and the surface radiation temperature [3,4], which was used to study surface evapotranspiration and soil water content, and further proposed a study of LST/vegetation index that is represented by the feature space.

The basic theory of the construction of the feature space depends on two aspects. First, there is a strong correlation between remote sensing vegetation index and LST [3–6];

* Corresponding author.

Presented at 2017 Qingdao International Water Congress, June 27–30, 2017, Qingdao, China.

Second, under the same fractional vegetation cover condition, when the crops were subjected to water stress, the leaf pores were self-confident and the vegetation transpiration was reduced, causing the LST to rise. Many scholars have studied the relationship between LST and vegetation index [7–11]. The results show that there is a strong negative correlation between them [3–6], and further studies show the relationship between LST/vegetation index and air temperature [12], soil water content [11,13], and so on. It is widely used for the estimation of surface parameters such as evapotranspiration [14,15] and soil water content [11], which is important for the study of agricultural irrigation, drought monitoring [16–19], land cover change monitoring, and water resources management and planning. The key to estimate the evapotranspiration and soil water content by using feature space is to determine the dry and wet edges, that is, to calculate the relationship between vegetation index and LST under sufficient water supply and extreme water shortages. Past research can be divided into two kinds of ideas, one is to rely on experience and prior knowledge, select the maximum LST on the dry edge [20,21], the main surface of the water surface temperature [22], the regional average temperature [23], or the minimum LST [20,21]. Another way is to calculate the LST or the temperature difference between the LST and the atmosphere at the vertex of the characteristic space by a certain principle [23–25]. For the construction of feature space, the determination of dry and wet edges is especially important, but the research on the fitting method of dry and wet edges is still relatively lacking.

In this paper, the fitting method of dry and wet edges of LST/vegetation index feature space is studied, the linear and index, logarithm, polynomial, and power functions are, respectively, used to fit the dry and wet edges, and the measured soil water content data were used to evaluate the fitting results, to explore and improve the applicability of the feature space method at large spatial scales.

2. Materials and methods

2.1. Study area

In this study, we selected a 158 km × 147 km area in Oklahoma, USA, with a center position of 36°2′12.48″N, 97°49′42.71″W, as shown in Fig. 1. The area is dominated by plains, and the altitude is between 252 and 592 m. The climate in the study area is dominated by dry continental climate. The annual average temperature is 15.5°C, and the rainfall is decreasing from east to west. Forest coverage is about 24%, mainly distributed in the eastern part of the region, the study area in the north of the main agricultural land, fractional vegetation cover is relatively low.

2.2. Remote sensing data

Through the US Geological Survey website (http://glovis.usgs.gov), download the Landsat-TM5 data of the study area, the imaging time is September 28, 2009, the image quality is the best grade, and no cloud cover. Landsat-TM5 contains visible light-thermal infrared multiple spectral channels and thermal infrared data, the spatial resolution of 30 m, the detailed parameters shown in Table 1.

2.3. Soil moisture data

Soil moisture data are from the NATIONAL INTEGRATED DROUGHT INFORMATION SYSTEM (https://www.drought.gov/drought/soil-moisture-map). The system contains a series of depth soil moisture and temperature, where the soil moisture measurement depth data include 5, 10, 20, 50, and 100 cm, and so on. There are 16 soil moisture observation stations in the study area (see Table 2 for details), and the spatial location of each site is shown in Fig. 1. In this paper, we use 5, 25, and 60 cm soil moisture content at three different depths to analyze the results of feature space calculation.

2.4. Soil type data

The soil type data are derived from the World Soil Database built by the Food and Agriculture Organization of the United Nations and the Vienna International Applied Systems Institute (Harmonized World Soil Database version 1.2) (http://webarchive.iiasa.ac.at/Research/LUC/External-World-soil-database). Through the query, in the study area, soil type is single Kastanozems soil. The soil type is rich in humus and is initially covered with precocious native grassland vegetation, which produces a brown surface layer in the first meter with a relatively high level of available calcium ions combined with soil particles and may have a thickness of 25–100 cm between the layers of stone.

2.5. Calculation of normalized difference vegetation index

In this study, the vegetation index of the characteristic space abscissa is selected using the most widely used

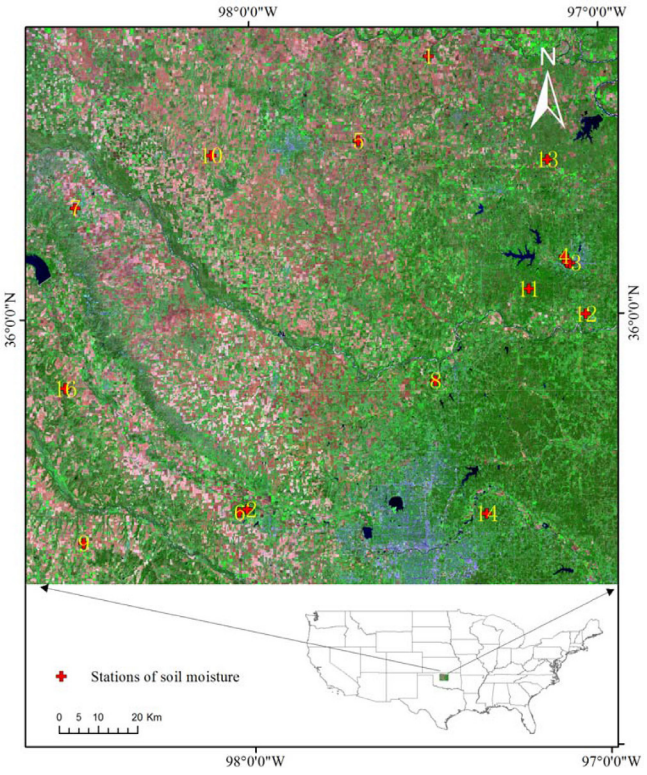

Fig. 1. Location map and soil moisture stations layout.

Table 1
The information of Landsat-TM5 data in the paper

Product ID	Multispectral	Thermal infrared	Spatial resolution (m)
LT50280352009271PAC01	Band 1 (Blue)	Band 6* (TIRS)	30
	Band 2 (Green)		30
	Band 3 (Red)		30
	Band 4 (NIR)		30
	Band 5 (SWIR1)		30
	Band 7 (SWIR2)		30

*The original spatial resolution of Band6 is 120 m, the product data used in this study are resampled and the spatial resolution is 30 m.
NIR, Near infrared; TIRS, thermal infrared remote sensing; SWIR, short wave infrared.

Table 2
The information of soil moisture stations

Number	Station ID	Station name	City	Latitude	Longitude
1	10209412	Breckinridge	Breckinridge	36.410000	–97.690000
2	10449412	El Reno	El Reno	35.550000	–98.040000
3	10479412	Fairview	Fairview	36.260000	–98.500000
4	10559412	Guthrie	Guthrie	35.850000	–97.480000
5	10589412	Hinton	Hinton	35.480000	–98.480000
6	10719412	Lahoma	Lahoma	36.380000	–98.110000
7	10759412	Marena	Coyle	36.060000	–97.210000
8	10999412	Perkins	Perkins	36.000000	–97.050000
9	11049412	Red Rock	Red Rock	36.360000	–97.150000
10	11129412	Spencer	Spencer	35.540000	–97.340000
11	11149412	Stillwater	Stillwater	36.120000	–97.100000
12	11279412	Watonga	Watonga	35.840000	–98.530000
13	60139612	Lamont (E13)	Lamont	36.605000	–97.485000
14	60189711	El Reno (E19)	El Reno	35.557000	–98.017000
15	70800212	Stillwater 2 W	Stillwater	36.118100	–97.091400
16	70810212	Stillwater 5 WNW	Stillwater	36.134600	–97.108200

WNW, West-northwest. It only represents a station name.

vegetation index—normalized difference vegetation index (NDVI). It has a good indicator of vegetation growth and spatial distribution, and has a strong correlation with fractional vegetation cover [26,27]. The mathematical expression is as follows:

$$\mathrm{NDVI} = \frac{\rho_{\mathrm{NIR}}\ \rho_{\mathrm{RED}}}{\rho_{\mathrm{NIR}} + \rho_{\mathrm{RED}}} \tag{1}$$

where ρ_{NIR} is for the near infrared band and ρ_{RED} is for the red band. The NDVI theoretical value is between –1 and 1. Negative values indicate that the ground is covered with clouds, water, snow, and other types, high reflectivity to visible light; zero value indicates that there are rock or bare soil and other types, near infrared band spectral value and red band spectral values are approximately equal; and positive values indicate fractional vegetation cover and increase with increasing coverage. However, due to the influence of surface humidity, solar lighting conditions, and atmospheric conditions, there are some abnormal values. In this study area, the negative value is mainly water body, and the masking is carried out when the feature space is constructed.

2.6. Calculation of LST

At present, the commonly used LST calculation method includes radiation transmission equation algorithm, single-channel algorithm, and split-window algorithm, predecessors for these three kinds of calculation methods carried out a series of studies [28]. The results show that the radiation transmission equation algorithm and split-window algorithm, the precision is relatively high, and the physical basis of the radiation transport equation algorithm is clear and the inversion precision is higher. Therefore, in this study, the radiation transport equation algorithm is selected to invert the LST. The principle is to estimate the effect of the atmosphere on the surface heat radiation and to reduce the effect of atmospheric heat radiation on the surface from the total amount of thermal radiation observed by the satellite sensor, to obtain the surface heat radiation intensity, and finally to heat radiation intensity into LST. The mathematical expression for LST calculation is as follows:

$$\mathrm{LST} = \frac{K_2}{\ln(1 + K_1\ /\ B(\mathrm{T}s))} \tag{2}$$

where K_1 and K_2 are the calibration constants of the sensor, B(Ts) refers to the black body radiation brightness of Ts, the mathematical expression of B(Ts) calculation is as follows:

$$L\lambda = (\varepsilon B(\mathrm{Ts}) + (1\varepsilon)L_{\downarrow})\tau + L_{\uparrow} \tag{3}$$

where $L\lambda$ is the thermal infrared radiation luminance value, ε is the radiant ratio of the surface, τ is the transmittance of the atmosphere in the hot infrared band, L↑ is effective bandpass upwelling radiance, and L↓ is effective bandpass downwelling radiance. Among them, the LST inversion of the atmosphere involved the band average atmospheric transmission, effective bandpass upwelling radiance, effective bandpass downwelling radiance can be obtained from NASA official website (http://atmcorr.gsfc.nasa.gov/). The surface emissivity is calculated using the NDVI threshold method proposed by Sobrino et al. [29]. The mathematical expression is as follows:

$$\varepsilon = 0.004 \times \mathrm{FVC} + 0.986 \tag{4}$$

where FVC refers to fractional vegetation cover. The fractional vegetation cover is calculated using the NDVI-based binary dichotomy model [26,30], and the mathematical expression is as follows:

$$\mathrm{FVC} = \left(\frac{\mathrm{NDVI}\ \mathrm{NDVI}_{\mathrm{soil}}}{\mathrm{NDVI}_{\mathrm{vegetation}}\ \mathrm{NDVI}_{\mathrm{soil}}} \right)^2 \tag{5}$$

where $\mathrm{NDVI}_{\mathrm{soil}}$ refers to the bare pixel values, and $\mathrm{NDVI}_{\mathrm{vegetation}}$ refers to the fractional vegetation cover of the pixel value.

2.7. Construction and verification of LST/NDVI feature space

The core of the LST/vegetation index feature space construction is the determination of dry and wet edges. The traditional method uses a linear fitting, that is, with a fixed NDVI interval cutting NDVI and LST scatter plot, respectively, to find the interval between the maximum and minimum LST, respectively, linear fitting NDVI value, get dry and wet side.

In this study, the same method is used to obtain the maximum and minimum values of LST, but the fitting method is in nonlinear relationship, it mainly includes index relations, linear relations, logarithm relations, polynomial relations, and power relations, as shown in Fig. 2. The mathematical expression of the linear fit is as follows:

$$\mathrm{LST}_{\mathrm{max/min}} = \begin{cases} \alpha \times \mathrm{NDVI} + \beta \\ \alpha \times \ln(\mathrm{NDVI}) + \beta \\ \alpha \times e^{\beta \times \mathrm{NDVI}} \\ \alpha \times \mathrm{NDVI}^{\beta} \\ \alpha_1 \times \mathrm{NDVI}^{n} + \alpha_2 \times \mathrm{NDVI}^{n-1} + \cdots + \alpha_n \times \mathrm{NDVI} + \alpha_0 \end{cases} \tag{6}$$

where α and β on behalf of the dry and wet edge fitting equations of the fitting coefficient.

Based on the LST/vegetation index feature space constructed by different function fitting methods, the soil water content of soil surface was calculated, and the mathematical expression was as follows:

$$\mathrm{LST/NDVI} = \frac{\mathrm{LST} - \mathrm{LST}_{\mathrm{min}}}{\mathrm{LST}_{\mathrm{max}} - \mathrm{LST}_{\mathrm{min}}} \tag{7}$$

LST/NDVI represents the soil water content, which is a dimensionless value between 0 and 1. Its value is closer to 1, representing the lower soil moisture content; the closer its value is to 0, the higher is the soil moisture content.

In order to evaluate the accuracy of the fitting of the LST/vegetation index feature space for different functions, the deterministic coefficient *r*-squared, root mean square error (RMSE) and mean absolute error (MAE) are used as the parameters to be evaluated in this study. The RMSE and MAE are mainly used to measure the deviation between the observed value and the model value, which can reflect the accuracy of the model calculation, the smaller the value, the higher the accuracy [30]. The mathematical expression is as follows:

$$\mathrm{RMSE} = \sqrt{\frac{\sum_i^n (\mathrm{X}_{\alpha,i} - \mathrm{X}_{\beta,i})^2}{n}} \tag{8}$$

$$\mathrm{MAE} = \frac{1}{n}\sum_{i=1}^{n} |(X_{\alpha,i} - X_{\beta,i})| \tag{9}$$

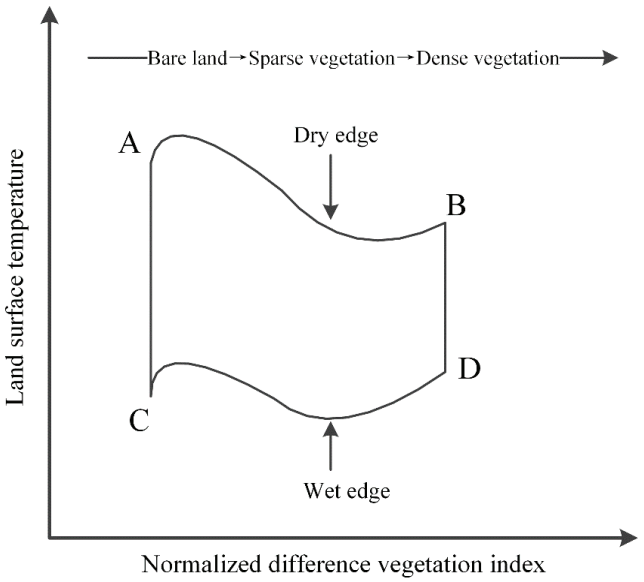

Fig. 2. Feature space of LST/NDVI, where Point A represents dry bare soil, low vegetation index, and high land surface temperature; B points on behalf of moist and dense vegetation, soil moist, and strong transpiration; C point represents wet bare soil, low vegetation index, and low land surface temperature; D points on behalf of dry lush vegetation, soil drought, and vegetation transpiration weak.

where $X_{\alpha,i}$ represents the true value, $X_{\beta,i}$ represents the calculated value of the model, and n represents the number of real values.

$$r^2 = \frac{\sum_{i=1}^{n}(P_i - \overline{P})(Q_i - \overline{Q})}{\sqrt{\sum_{i=1}^{n}(P_i - \overline{P})^2 \cdot \sum_{i=1}^{n}(Q_i - \overline{Q})^2}} \tag{10}$$

where P and Q are the measured and estimated values, respectively; $\overline{P}$ and $\overline{Q}$ are the mean of the measured and estimated values, respectively; the subscript i represents n measured values or the i-th value in the estimate.

3. Results and discussion

3.1. Analysis of NDVI and LST calculation results

NDVI and LST are two key parameters for LST/vegetation index feature space. Where NDVI is the abscissa of the feature space, and LST is the ordinate of the feature space. In this study, using the Landsat TM5 satellite remote sensing image data, the NDVI was calculated by combining Eq. (1) after atmospheric correction and radiometric calibration, and the LST was calculated by Eqs. (2)–(5), and its statistics are carried out by means of the ENVI software platform. The results are shown in Figs. 3 and 4.

From Fig. 3(a), we can see that the spatial distribution of NDVI values in the study area is quite different. In the central and northern regions, the NDVI values are concentrated around 0.15, and the high vegetation index and low vegetation index mosaic distribution characteristics; in the eastern region of the main forest cover area, NDVI value is mainly concentrated in 0.55 or so. According to the NDVI statistical curve in the study area (Fig. 3(b)), the NDVI values in the study area are mainly concentrated between 0.1 and 0.8, and the number of the maximum and the minimum is relatively small; and the number of NDVI values is 0.1–0.16 and 0.32–0.55 showed increasing trend in the two intervals, and there was a decreasing trend in the range of 0.16–0.32 and 0.55–0.9. The above results show that the change of surface cover from bare soil to sparse vegetation to dense vegetation is reflected in the whole study area, which satisfies the requirement that the vegetation has different coverage.

It can be seen from Fig. 4(a) that the LST value in the eastern part of the study area is relatively low, mainly in the range of 20°C–25°C, and the LST value in the middle and northern regions is relatively high, mainly in the range of 25°C–35°C, and the LST values of the two intervals of 25°C–30°C and

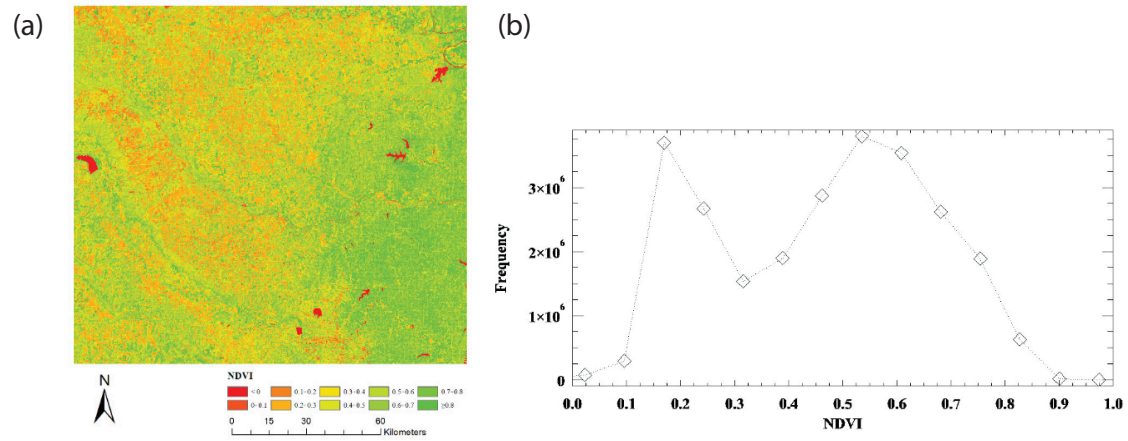

Fig. 3. NDVI calculation results: (a) NDVI spatial distribution and (b) NDVI value statistics.

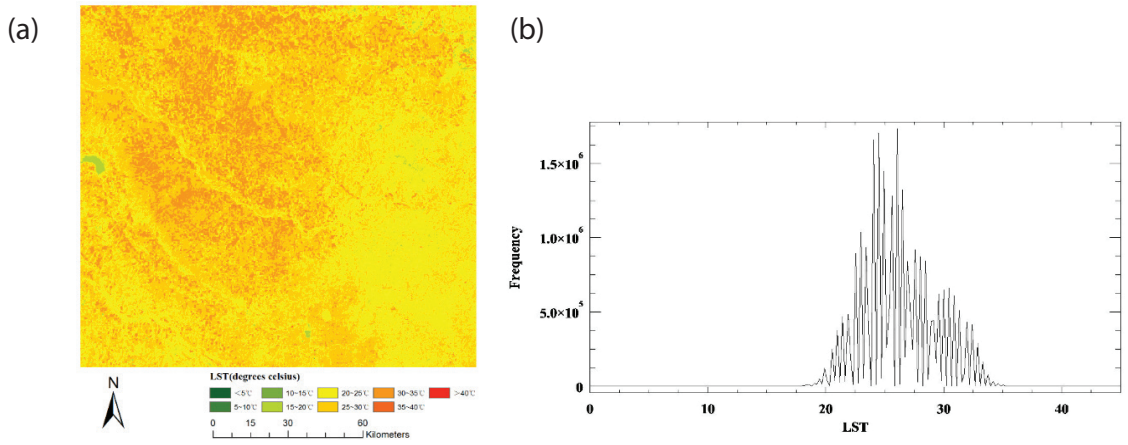

Fig. 4. LST calculation results: (a) LST spatial distribution and (b) LST value statistics.

30°C–35°C show the characteristics of mosaic distribution. According to the LST value of the study area (Fig. 4(b)), the LST values in the study area are mainly concentrated between 20°C and 35°C, while the number of LST values less than 20°C and greater than 35°C is relatively small, and the range of variation of LST value is wide, which can meet the requirements of the LST change range which requires sufficient range of feature space. Therefore, the calculated NDVI and LST can meet the requirements of constructing the LST/vegetation index feature space, and further construct the feature space based on the above two parameters for dry and wet edge fitting.

3.2. Dry and wet edges fitting and LST/NDVI feature space construction

Based on the ENVI software platform, the maximum and minimum values of NDVI corresponding to LST are calculated by spatial superposition analysis. The results are shown in Fig. 5. On the dry side, that is, the discrete surface composed of the largest LST, NDVI, and LST showing a non-linear relationship, and NDVI for 0.3–0.7 range of non-linear characteristics of the relationship between the performances is particularly evident. On the wet side, that is, the discrete surface of the minimum LST, NDVI between 0 and 0.8, LST increases with the increase of NDVI, but after more than 0.8, LST value is basically stable, mainly due to high fractional vegetation cover area, when the NDVI reaches a certain value after the occurrence of saturation phenomenon, which Wang et al. [31] consistent with the results of the study.

The dry and wet edges in Fig. 5 are fitted by linear, polynomial, logarithm, index, and power functions, and the deterministic coefficient *r*-squared is calculated using Eq. (10). The results are shown in Table 3.

The deterministic coefficient *r*-squared of the five different functions is between 0.4 and 0.7, as shown in Table 3. For the dry edge, the polynomial function is the best fit, *r*-squared is 0.67, followed by the index function, *r*-squared is 0.64, logarithm function and power function fitting effect is relatively poor, both *r*-squared are not more than 0.5. For the wet edge, the polynomial fitting has the best effect, *r*-squared is 0.7, the power function is the second, the index function is the worst. Integrated dry and wet edges of the fitting method, the polynomial function has the best-fitting effect.

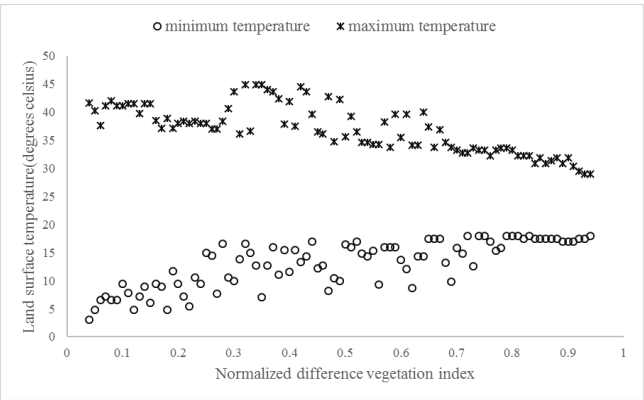

Fig. 5. Construction of LST/NDVI feature space in the study area.

3.3. Feature space calculation and verification analysis

According to the equations of the linear and polynomial, logarithm, index, and power of the five functions on the dry and wet edges, as shown in Table 3, and using Eqs. (1) and (2), the LST/NDVI is calculated by combining the NDVI data and the LST data (Fig. 4), and the results are shown in Fig. 6.

The results of the LST/NDVI in Fig. 6 show that the fitting of the five functions can reflect the spatial distribution of soil moisture, and from the macroscopic point of view, the spatial distribution of the difference is small, and the areas with low soil water content are mainly concentrated in the middle and north of the study area, and areas with relatively high soil water content are concentrated in the eastern part of the study area. But for the performance of local areas, five kinds of functions are different. The results of the index function are mainly concentrated between 0.5 and 0.6, and the results of the linear function are mainly concentrated between 0.45 and 0.55, and the spatial distribution of the data is consistent with the index function. The logarithm function is mainly concentrated in the range of 0.55–0.6, and the spatial mutation in the range of 0.2–0.4 is more obvious than the index function, linear function and power function. And the calculation results of the power function are mainly concentrated in 0.6 or so, and the numerical change in the range of 0.2–0.6 shows a gentle upward trend, and there is no obvious mutation linearity. And the results of the polynomial function are obvious in the range of 0.2–0.8, and the data are mainly concentrated in the range of 0.4–0.6. Because most of the northern part of the study area is the characteristic of mosaic distribution for agricultural land, high vegetation area and low vegetation area, so it is easy to cause the results of the phenomenon of mutation, and the result of the polynomial function is more in line with the above characteristics.

The LST/NDVI results of the feature space calculation (Fig. 6) were calculated by using the index function, the linear function, the polynomial function, the logarithmic function, and the power function, respectively. The spatial analysis module of ArcGIS software platform was used to extract the LST/NDVI, the results of soil and moisture content were compared with the measured data of soil moisture content, and the RMSE and MAE parameters were used to analyze the accuracy of the calculation results.

Table 3
Five function fitting equations of dry and wet edges and their *r*-squared

Functions	Fitting equations	r^2
Index	Dry: $y = 43.441e^{-0.344x}$	0.64
	Wet: $y = 7.0404e^{1.1286x}$	0.59
Linear	Dry: $y = -12.273x + 42.965$	0.60
	Wet: $y = 12.564x + 6.9277$	0.63
Polynomial	Dry: $y = -18.473x^2 + 5.8303x + 39.804$	0.67
	Wet: $y = -568.27x^5 + 1{,}340x^4 - 1{,}095.1x^3 + 345.83x^2 - 14.619x + 5.456$	0.70
Logarithm	Dry: $y = -3.568 \ln(x) + 33.633$	0.41
	Wet: $y = 4.5004 \ln(x) + 17.268$	0.67
Power	Dry: $y = 33.493x^{-0.099}$	0.43
	Wet: $y = 18.282x^{0.4303}$	0.69

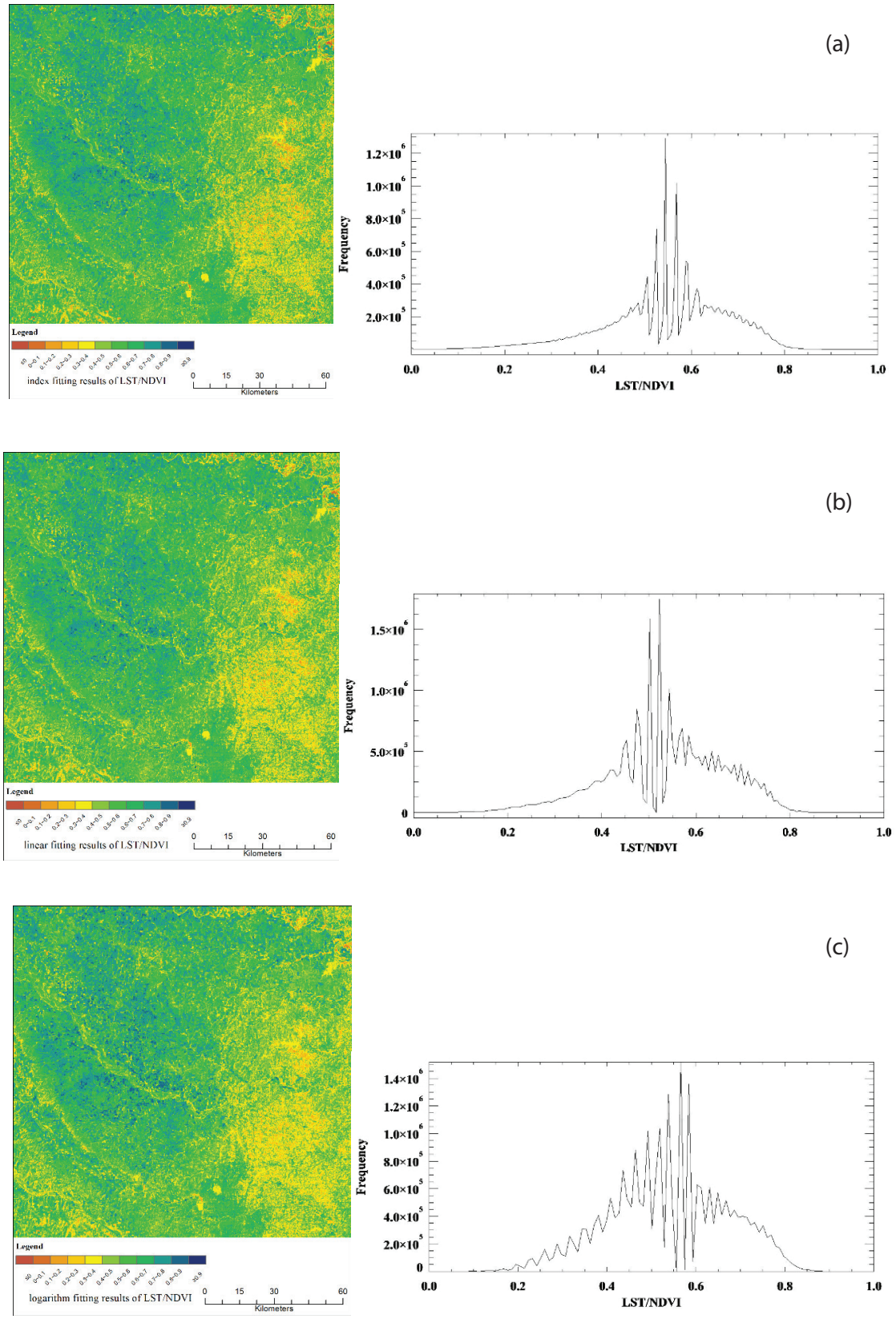

Fig. 6. LST/NDVI calculation results of five function fitting equations in the study area: (a) index fitting results of LST/NDVI (left) and spatial distribution of data values (right); (b) linear fitting results of LST/NDVI (left) and spatial distribution of data values (right); (c) logarithm fitting results of LST/NDVI (left) and spatial distribution of data values (right);

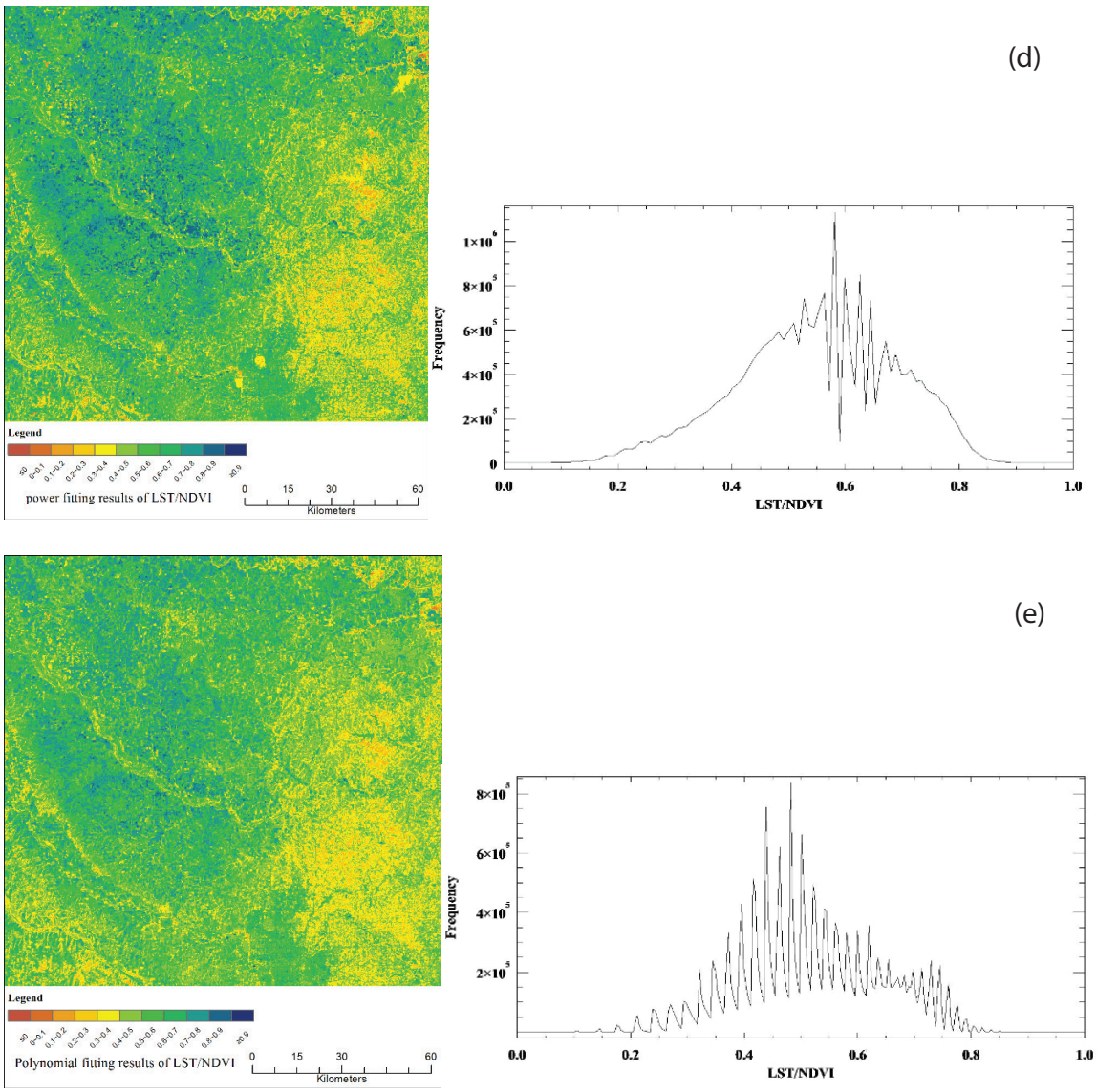

Fig. 6 (Continued). (d) power fitting results of LST/NDVI (left) and spatial distribution of data values (right); and (e) polynomial fitting results of LST/NDVI (left) and spatial distribution of data values (right).

Because the soil type in the study area is Kastanozems soil, the soil type is single, so it cannot consider the influence of different soil types. Soil moisture content is the volume of water content, the model calculation results for the relative water content, without considering the soil texture and other factors, there is a proportional relationship between the two studies show that there is a certain correlation between them, it can be used as a precision evaluation reference [11,16,18,32]. The observed data of the 16 soil moisture sites obtained in this study included the soil moisture content of three different depths of 5, 25, and 60 cm. The three groups of data at different depths of 16 soil moisture sites were fitted with five functions. The results are compared and the RMSE and MAE are calculated. The results are shown in Table 4.

Table 4
RMSE and MAE calculation results of five function fitting equations

Functions	RMSE			MAE		
	5 cm	25 cm	60 cm	5 cm	25 cm	60 cm
Index	0.33	0.30	0.32	0.31	0.27	0.30
Linear	0.31	0.29	0.30	0.29	0.26	0.28
Polynomial	0.32	0.29	0.31	0.29	0.26	0.28
Logarithm	0.29	0.27	0.28	0.26	0.23	0.25
Power	0.33	0.31	0.32	0.30	0.27	0.30

According to Table 4, we can see that there are some differences in the accuracy of the results of the five function fitting dry and wet edges. It can be seen from the results of RMSE that the value of the polynomial function is 0.29, the linear function is 0.31, the logarithm function is 0.32, the index function and the power function are both 0.33 and 25 cm. The results show that the value of the polynomial function is 0.27, followed by the linear function and the logarithm function, both 0.29, the index

function is 0.30, the power function is 0.31, and the soil water content is 60cm, The polynomial function has a minimum value of 0.28, followed by a linear function of 0.30, a logarithm function of 0.31, a power function and an index function of 0.32. From the results of the MAE, it can be seen that the MAE values of the five functions are the smallest for the five different depths of 5, 25, and 60 cm, which are 0.26, 0.23 and 0.25, respectively, and the minimum value is obtained at 25 cm depth.

4. Conclusions

At present, the research on the different fitting methods of dry and wet edges is still lacking. In view of the shortcomings of the traditional LST/vegetation index triangular or trapezoidal feature space, and five different functions are used to fit the dry and wet edges of the feature space, and combined with field observation site data on the Oklahoma, United States, were applied, the results show the following:

The dry edges of LST and NDVI constructed in the feature space are more likely to be polynomial distribution, and the *r*-squared fitted in the polynomial is the highest in the five fitting modes, reaching 0.67. The wet edges of LST and NDVI constructed in the feature space are more likely to be polynomial distributions, and the *r*-squared fitted in the polynomial is the highest in the five fitting modes, reaching 0.70.

The five functions of linear, polynomial, logarithm, index, and power are used to fit the dry and wet edges, and the polynomial fitting method works best, *r*-squared are more than 0.66. At the same time, the comparative analysis of soil water content in the study area showed that the RMSE and MAE of polynomial fitting were the smallest, which were 0.27 and 0.23, and it is shown that the water content of the soil surface is closest to the real value based on the polynomial fitting of the dry and wet edges inversion.

For an optimal fitting method, it is necessary to find an optimal solution between fitting accuracy and fitting efficiency. And in the course of this paper, the precision of the dry and wet edges is mainly given priority, because the amount of data involved is not large, and the time cost of the computer calculation process is not taken into account. But for the operation of large amounts of data, in the practical application process need to consider the time efficiency, which is the next step need to study the problem.

Acknowledgements

Research funded by the Guangdong Province water conservancy science and technology innovation project -titled "Study on Estimation Method of Effective Utilization Coefficient of Irrigation Water Based on Remote Sensing Evapotranspiration Model" (2016-09). The authors also wish to thank the anonymous reviewers for their valuable and useful suggestions that clearly improved this paper.

References

[1] J.C. Price, Using spatial context in satellite data to infer regional scale evapotranspiration, IEEE Trans. Geosci. Remote Sens., 28 (1990) 940–948.
[2] T. Carlson, An overview of the "Triangle Method" for estimating surface evapotranspiration and soil moisture from satellite imagery, Sensors, 7 (2007) 1612–1629.
[3] S.N. Goward, G.D. Cruickshanks, A.S. Hope, Observed relation between thermal emission and reflected spectral radiance of a complex vegetated landscape, Remote Sens. Environ., 18 (1985) 137–146.
[4] R.R. Nemani, S.W. Running, Estimation of regional surface resistance to evapotranspiration from NDVI and thermal-IR AVHRR data, J. Appl. Meteorol., 28 (1989) 276–284.
[5] S. Goward, A. Hope, Evapotranspiration from combined reflected solar and emitted terrestrial radiation: preliminary FIFE results from AVHRR data, Adv. Space Res., 9 (1989) 239–249.
[6] T.N. Carlson, E.M. Perry, T.J. Schmugge, Remote estimation of soil moisture availability and fractional vegetation cover for agricultural fields, Agric. For. Meteorol., 52 (1990) 45–69.
[7] R. Nemani, L. Pierce, S. Running, Developing satellite-derived estimates of surface moisture status, J. Appl. Meteorol., 32 (1993) 548–557.
[8] T.N. Carlson, R.R. Gillies, E.M. Perry, A method to make use of thermal infrared temperature and NDVI measurements to infer surface soil water content and fractional vegetation cover, Remote Sens. Rev., 9 (1994) 161–173.
[9] R. Gillies, W. Kustas, K. Humes, A verification of the 'triangle' method for obtaining surface soil water content and energy fluxes from remote measurements of the Normalized Difference Vegetation Index (NDVI) and surface e, Int. J. Remote Sens., 18 (1997) 3145–3166.
[10] E. Boegh, H. Soegaard, N. Hanan, P. Kabat, L. Lesch, A remote sensing study of the NDVI–T_s relationship and the transpiration from sparse vegetation in the Sahel based on high-resolution satellite data, Remote Sens. Environ., 69 (1999) 224–240.
[11] I. Sandholt, K. Rasmussen, J. Andersen, A simple interpretation of the surface temperature/vegetation index space for assessment of surface moisture status, Remote Sens. Environ., 79 (2002) 213–224.
[12] L. Prihodko, S.N. Goward, Estimation of air temperature from remotely sensed surface observations, Remote Sens. Environ., 60 (1997) 335–346.
[13] J.A. Otkin, M.C. Anderson, C.R. Hain, M.D. Svoboda, D.K. Johnson, R. Mueller, T. Tadesse, B.D. Wardlow, J. Brown, Assessing the evolution of soil moisture and vegetation conditions during the 2012 United States flash drought, Agric. For. Meteor., 218–219 (2016) 230–242.
[14] S. Stisen, I. Sandholt, A. Nørgaard, R. Fensholt, K.H. Jensen, Combining the triangle method with thermal inertia to estimate regional evapotranspiration—applied to MSG-SEVIRI data in the Senegal River basin, Remote Sens. Environ., 112 (2008) 1242–1255.
[15] M. Minacapilli, S. Consoli, D. Vanella, G. Ciraolo, A. Motisi, A time domain triangle method approach to estimate actual evapotranspiration: application in a Mediterranean region using MODIS and MSG-SEVIRI products, Remote Sens. Environ., 174 (2016) 10–23.
[16] J. Zhao, J. Xu, X. Xie, H. Lu, Drought monitoring based on TIGGE and distributed hydrological model in Huaihe River Basin, China, Sci. Total Environ., 553 (2016) 358–365.
[17] T. Zhang, X. Lin, Assessing future drought impacts on yields based on historical irrigation reaction to drought for four major crops in Kansas, Sci. Total Environ., 550 (2016) 851–860.
[18] J. Martínez-Fernández, A. González-Zamora, N. Sánchez, A. Gumuzzio, C.M. Herrero-Jiménez, Satellite soil moisture for agricultural drought monitoring: assessment of the SMOS derived Soil Water Deficit Index, Remote Sens. Environ., 177 (2016) 277–286.
[19] T.J. Assal, P.L. Anderson, J. Sibold, Spatial and temporal trends of drought effects in a heterogeneous semi-arid forest ecosystem, Forest Ecol. Manage., 365 (2016) 137–151.
[20] T.N. Carlson, R.R. Gillies, T.J. Schmugge, An interpretation of methodologies for indirect measurement of soil water content, Agric. For. Meteor., 77 (1995) 191–205.
[21] L. Jiang, S. Islam, A methodology for estimation of surface evapotranspiration over large areas using remote sensing observations, Geophys. Res. Lett., 26 (1999) 2773–2776.
[22] L. Jiang, S. Islam, W. Guo, A.S. Jutla, S.U.S. Senarath, B.H. Ramsay, E. Eltahir, A satellite-based Daily Actual

Evapotranspiration estimation algorithm over South Florida, Global Planet. Change, 67 (2009) 62–77.
[23] D. Long, V.P. Singh, A modified surface energy balance algorithm for land (M-SEBAL) based on a trapezoidal framework, Water Resour. Res., 48 (2012). doi: 10.1029/2011WR010607.
[24] M. Moran, T. Clarke, Y. Inoue, A. Vidal, Estimating crop water deficit using the relation between surface-air temperature and spectral vegetation index, Remote Sens. Environ., 49 (1994) 246–263.
[25] A. Karnieli, N. Agam, R.T. Pinker, M. Anderson, M.L. Imhoff, G.G. Gutman, N. Panov, A. Goldberg, Use of NDVI and land surface temperature for drought assessment: merits and limitations, J. Clim., 23 (2010) 618–633.
[26] Y. Liu, X. Mu, H. Wang, A novel method for extracting green fractional vegetation cover from digital images, J. Veg. Sci., 23 (2012) 406–418.
[27] X. Zhang, C. Liao, J. Li, Q. Sun, Fractional vegetation cover estimation in arid and semi-arid environments using HJ-1 satellite hyperspectral data, Int. J. Appl. Earth Obs. Geoinf., 21 (2013) 506–512.
[28] J. Bai, S. Liu, G. Hu, Inversion and verification of land surface temperature with remote sensing TM/ETM+ data, Trans. CSAE, 24 (2008) 148–154 (in Chinese with English abstract).
[29] J.A. Sobrino, J.C. Jiménez-Muñoz, L. Paolini, Land surface temperature retrieval from LANDSAT TM 5, Remote Sens. Environ., 90 (2004) 434–440.
[30] P.E. Dennison, D.A. Roberts, Endmember selection for multiple endmember spectral mixture analysis using endmember average RMSE, Remote Sens. Environ., 87 (2003) 123–135.
[31] X.H. Wang, P.T. Cong, C.Q. Liu, et al., Analysis of vegetation variation and stress factors in the Pearl River basin from 2004 to 2013, Acta Ecol. Sinica, 37 (2017) 6494–6503.
[32] D. Liu, A.K. Mishra, Z. Yu, Evaluating uncertainties in multi-layer soil moisture estimation with support vector machines and ensemble Kalman filtering, J. Hydrol.,538 (2016) 243–255.